Received 29 November 2016; revised 20 January 2017 and 3 March 2017; accepted 4 March 2017. Date of publication 7 March 2017; date of current version 24 April 2017. The review of this paper was arranged by Editor J. Kumar.

Digital Object Identifier 10.1109/JEDS.2017.2679209

Quantum-Mechanical Analysis of Amorphous Oxide-Based Thin-Film Transistors

JAEWOOK JEONG

School of Information and Communication Engineering, Chungbuk National University, Cheongju 362-763, South Korea

CORRESPONDING AUTHOR: J. JEONG (e-mail: jjeong@cbnu.ac.kr)

This work was supported in part by the National Research Foundation of Korea Grant funded by the Korean Government under Grant NRF-2014R1A2A2A01006588, in part by the Ministry of Science, ICT, and Future Planning of Korea under the Information Technology Research Center Support Program Supervised by the Institute for Information and Communications Technology Promotion under Grant IITP-2016-R0992-16-1008, and in part by the "Human Resources Program in Energy Technology" of the Korea Institute of Energy Technology Evaluation and Planning through the Ministry of Trade, Industry and Energy, South Korea under Grant 20164030201330.

ABSTRACT In this paper, we analyzed the electrical characteristics of amorphous oxide-based thin-film transistors (TFTs) with extremely thin active layers using a quantum-mechanical method (density gradient method) and a technology computer-aided design simulator. We observed that the evaluation of the TFT performance using the classical method resulted in errors, especially, when the interfacial-defect density of states was high. The electrical characteristics of the TFTs are influenced differently by the bulk and interfacial states when the quantum-mechanical effect is considered. Therefore, it is essential to apply the quantum effect to analyze the electrical characteristics of amorphous oxide-based TFTs with extremely thin active layers.

INDEX TERMS a-IGZO, thin-film transistor, quantum, threshold voltage shift, simulation.

I. INTRODUCTION

Amorphous oxide-based thin-film transistors (TFTs) have been widely investigated theoretically and experimentally and are considered to be promising candidates to replace conventional amorphous silicon and poly-silicon-based TFTs [1]–[3]. To evaluate the performance of oxide-based TFTs, numerical simulations have been used, particularly for understanding the roles of donor- and acceptor-like defect states in an active layer [4]–[7]. Until now, the device simulations have been performed on the assumption that the electrons are classical particles that obey classical electrodynamics. This assumption is precise if the active layer thickness is higher than tens of nanometers. However, recent developments in the fabrication of oxide-based TFTs allow the reduction of the active layer thickness to below 5 nm for vacuum- and solution-processed oxide-based TFTs [8], [9]. When the active layer thickness of a crystalline transistor is in the nanometer scale, quantum-mechanical effects must be considered to analyze the electrical characteristics of electrons in the active layer. For the conventional metal–oxide-semiconductor field-effect transistor (MOSFET), quantum effects induce an increase in the effective thickness of the gate insulator [10]. In this case, the quantum effect becomes prominent only when the gate insulator is thin because the variation of the effective thickness of the gate insulator is in the order of nanometers. Therefore, we can predict that the quantum effect is negligible for oxide-based TFTs because the thickness of the gate insulator is over 100 nm for conventional amorphous-based TFTs. However, these TFTs do contain a significant defect density of states (DOS) in the active layer. The device performance is influenced by both the interfacial-defect density and the bulk-defect density. To further evaluate the performance of amorphous oxide-based TFTs using the quantum effect, the interfacial defect density and the bulk-defect density were considered separately.

In this study, we examined the variations in the performance of oxide-based TFTs with thin active layers by considering the quantum effect using a technology-aided design (TCAD) simulator from Silvaco Inc. The density gradient method, which is one of the important methods applied to analyze this effect, was used to evaluate the importance of quantum effects in the active layer.

2168-6734 © 2017 IEEE. Translations and content mining are permitted for academic research only.
Personal use is also permitted, but republication/redistribution requires IEEE permission.
See http://www.ieee.org/publications_standards/publications/rights/index.html for more information.

II. QUANTUM EFFECT IN AMORPHOUS MATERIALS

The electronic band structure of amorphous semiconductors is typically assumed to be similar to that of crystalline semiconductors. Even in the amorphous phase, it exhibits conduction and valence bands with a continuous distribution of defect DOS in the bandgap region. Compared to crystalline semiconductors with discrete defect levels, the defect DOS in amorphous materials is typically modeled using continuous Gaussian and exponentially decaying functions in the bandgap region. Owing to the similarity of the band structure, the quantum confinement effect in amorphous materials has been extensively investigated using amorphous silicon (a-Si) semiconductors. The quantum confinement effect in a-Si has been directly observed as blue shifts in photoluminescence when the dot size decreases to the nanometer scale. Despite the presence of a significant number of defect states, blue shifts have been observed in the photoluminescence of a-Si quantum dots, which indicated that the electrons in the conduction band obey quantum mechanics [11]–[13]. In this case, the question arises as to how the quantum effect can be applied to trapped and free electrons. This question has been answered by Allan *et al.* [14]. The electronic states of a-Si are categorized into three groups: extended states (free electron), weakly localized states (trapped electron that can be easily delocalized), and strongly localized states (trapped electron). It has been observed that among these three groups, the electrons in the extended and weakly localized states contribute the blue shifts in the photoluminescence of quantum dots, whereas the electrons in strongly localized states do not. Therefore, these results can be applied in the simulation, where the electrical characteristics of free and trapped electrons are determined using quantum and classical methods, respectively. The same method is applied to amorphous oxide-based TFTs, as they have a similar band structure with a-Si-based TFTs, which includes conduction and valence bands as well as a continuous distribution of defect states in the bandgap region. The calculation procedure begins with evaluating the electrical properties using the classical method. Then, the quantum effect is applied by adding the quantum potential of the density gradient method in the drift-diffusion equation, which will be discussed in Section III.

III. DENSITY-GRADIENT THEORY

We considered only electron transport because oxide-based TFTs are mainly influenced by electron conduction. The Schrödinger equation is the central equation that must be solved to evaluate the quantum effect. The direct calculation of the Schrödinger equation is possible using the Schrödinger–Poisson model [15], [16]. However, the method is inefficient for the application of various types of device simulation owing to the long calculation time. However, the density-gradient theory, which is derived from the Schrödinger equation, can be used to calculate the quantum effect of MOSFETs efficiently [17], [18]. In this case, we have an additional quantum potential factor, which is defined by the following equation:

$$\Lambda = -\frac{h^2}{6m_e}\frac{\nabla^2\sqrt{n}}{\sqrt{n}} \tag{1}$$

Here, n is the electron density, h is the Plank constant, m_e is the effective mass of the electron, and q is the elementary charge. Using Eq. (1), the classical drift-diffusion model is modified by the following equation:

$$\vec{J} = -qD_n\nabla n - qn\mu_n\nabla(\phi - \Lambda) \tag{2}$$

Here, D_n is the diffusion constant and μ_n is the mobility. It is shown that the quantum potential term is included in the drift part of Eq. (2). Moreover, Eq. (1) indicates that if there is a large gradient of electron density (for example, at the interface between an insulator and a semiconductor), there is an imaginary force that impels the electron from the interface. When the quantum effect is considered, the performance of amorphous oxide-based TFTs is accurately analyzed by combining the density-gradient theory and the defect density of states model. In conventional MOSFETs, the effect of defects or impurities on the device performance has been examined by applying the density gradient method, concurrently [19]. When the defect DOS is considered, the Poisson equation, including the quantum potential, can be expressed using the following equation:

$$\nabla \bullet (\varepsilon\nabla\psi) = -q\left(p - n + N_D^+ - N_A^-\right) \tag{3}$$

$$\phi_n = \psi - \frac{kT}{q}\ln\frac{n}{n_i} - \Lambda \tag{4}$$

Here, ε is the permittivity of the semiconductor layer, φ_n is the quasi-Fermi potential, k is the Boltzmann constant, and N_D^+ and N_A^- are the ionized donor- and acceptor-like defect densities, respectively. By solving Eqs. (1)–(4) self-consistently, the electrical characteristics can be simulated; this approach is implemented in TCAD simulators. The difference between MOSFETs and TFTs is the distribution of the defect DOS. As discussed in Section IV, it is important to determine the distribution function of the defect states due to the continuous defect DOS of TFTs.

IV. DEVICE STRUCTURE AND DENSITY OF STATES

Among the various amorphous oxide-based TFTs, the amorphous indium–gallium–zinc-oxide TFT (a-IGZO TFT) is the most important and representative device owing to its excellent electrical and optical properties [20], [21]. Therefore, the material parameters of a-IGZO TFT were used to simulate the active layer. Figure 1 shows the a-IGZO TFT structure used in this study. We assumed the thickness of the gate insulator (SiO_x) and the active layer (a-IGZO) to be 200 and 5 nm, respectively. The channel length (L) was 5 μm and the passivation layer covered the entire back channel region. In Eq. (1), m_e was assumed to be 0.34m_f (m_f is the electron mass in free space), which has been previously determined by measuring the Burstein–Moss shift of the optical absorption spectrum [22]. To simulate the a-IGZO TFT, both the

TABLE 1. Bulk and interfacial DOS of the reference TFTs used in this study.

Parameter	Bulk-defect DOS (reference)		Interfacial-defect DOS (reference)	
	Value	Unit	Value	Unit
W_{TA}	0.18	eV	0.18	eV
N_{TA}	3.5×10^{18}	$cm^{-3}eV^{-1}$	1.8×10^{12}	$cm^{-2}eV^{-1}$
W_{GA}	0.21	eV	0.21	eV
N_{GA}	1.6×10^{17}	$cm^{-3}eV^{-1}$	8.0×10^{10}	$cm^{-2}eV^{-1}$
E_{GA} (from E_C)	1.34	eV	1.34	eV

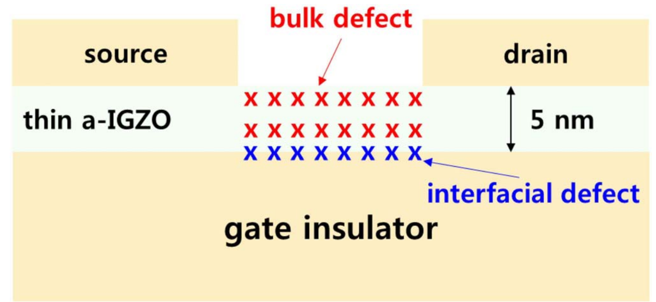

FIGURE 1. a-IGZO TFT structure used in this study.

interfacial- and bulk-defect DOSs were considered. The simulations of the bulk and interfacial defects were performed separately to distinguish the effect originating from each defect DOS. The model contains four distribution functions: the conduction band tail function (NA_{tail}), the conduction band deep function (NA_{deep}), the valence band tail function (ND_{tail}), and the valence band deep function (ND_{deep}) in the bandgap region. Among these four, we considered the two functions of acceptor-like states that mainly influence the electron current. Each function is described for the bulk and interfacial states as follows:

$$NA_{tail_bulk}(E) = N_{TA_bulk}\exp\left[-(E_C - E)/W_{TA_bulk}\right], \quad (5)$$

$$NA_{deep_bulk}(E) = N_{GA_bulk}\exp\left[-(E - E_{GA})^2/W^2_{GA_bulk}\right], \quad (6)$$

$$NA_{tail_int}(E) = N_{TA_int}\exp\left[-(E_C - E)/W_{TA_int}\right], \quad (7)$$

$$NA_{deep_int}(E) = N_{GA_int}\exp\left[-(E - E_{GA})^2/W^2_{GA_int}\right], \quad (8)$$

where E_C is the conduction band energy, N_{TA} is the peak value of the conduction band tail states, W_{TA} is the conduction band characteristic energy, N_{GA} is the peak value of the conduction band deep states, W_{GA} is the variance of the conduction band deep states, and E_{GA} is the mean energy level of the conduction band deep states. The subscripts "bulk" and "int" in Eqs. (1)–(4) denote the bulk and interfacial states, respectively. The parameters of Eqs. (1) and (2) were determined from previously reported results [23]. Because the thickness of the active layer in [23] is 10 times higher than that considered in this study, we set the N_{TA} and N_{GA} values of the reference device as shown in Table 1, namely, 10 times larger than those of [23]. The interfacial-defect DOS was evaluated on the assumption that all the bulk defects were located on the active/gate insulator interface with the same distribution function, as shown in Fig. 1. Therefore, the N_{TA_int} and N_{GA_int} values were calculated by $N_{TA_int} = t \times N_{TA_bulk}$ and $N_{GA_int} = t \times N_{GA_bulk}$, where t is the thickness of the active layer. The reference parameters are summarized in Table 1.

V. EFFECTS OF BULK DENSITY OF STATES

Figure 2(a) shows the resulting quantum potential distribution in the active layer along the thickness direction when the bulk-defect DOS is considered (the interfacial-defect DOS is assumed to be zero). From Eq. (1), the quantum potential is proportional to the Laplacian of the electron density. Therefore, the quantum potentials at the active/gate insulator and active/passivation interfaces are large. As the gradient of the quantum potential is the strength of the electric field, it induces a force that repulses electrons from the back and front interfaces to the center of the active layer. As shown in Fig. 2(b), this leads to a shift of the free electron density (n_e) distribution.

When the quantum effect is considered, the peak point of the electron density is not in the active/gate insulator interface but separated from the front interface. As shown in Fig. 2(d), the main current path is formed apart from the interface region because an electron channel is formed in the high-electron-density channel region. Figure 2(c) shows the trapped electron density (n_t). Unlike the free electron density distribution, the trapped electron density shows nearly the same distribution for the classical and quantum mechanical methods because the trapped electrons are localized in defect sites.

Figures 3(a) and (b) show the transfer characteristics of a-IGZO TFTs operating in the linear region ($V_{DS} = 0.01$ V) for various bulk-defect DOSs. The bulk-defect DOS varied from 1 to 10 times the reference value. The resulting transfer curve reveals no difference between the results of the classical and quantum-mechanical methods. As a spatially uniform distribution is assumed for the bulk-defect DOS in the active region and the total numbers of free electrons from the classical and quantum-mechanical calculations are similar, no difference is observed in the drain current in this case.

Figure 3(c) shows the transfer characteristics of a-IGZO TFTs operating in the saturation region ($V_{DS} = 20$ V) for various bulk-defect DOSs. In the saturation region, the central equation describing the current–voltage characteristics is expressed as $I_{DS} = \mu C_{OX} W (V_{GS} - V_{TH})^2/2L$, where μ is the electron mobility, C_{OX} is the capacitance of the gate insulator per unit area, V_{TH} is the threshold voltage, and W is the channel width. Consequently, the relation between $I_{DS}^{1/2}$ and V_{GS} is linear and its slope and x-intercept denote the field-effect mobility and V_{TH}, respectively. Figure 3(d) shows the $I_{DS}^{1/2}$ *vs.* V_{GS} graph for various bulk-defect DOSs. Unlike the case of linear region operation, a slight positive shift is observed in V_{TH} without varying the field-effect mobility when the quantum-mechanical calculation is applied. However, the amount of the shift in the threshold voltage does not depend

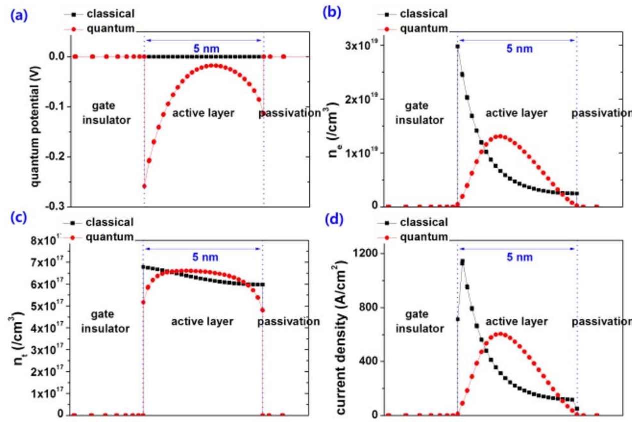

FIGURE 2. Electrical characteristics of an a-IGZO TFT when $V_{GS} = 20$ V and $V_{DS} = 0.01$ V: (a) quantum potential, (b) electron density distribution, (c) trapped electron density in acceptor-like defect states, and (d) current density distribution.

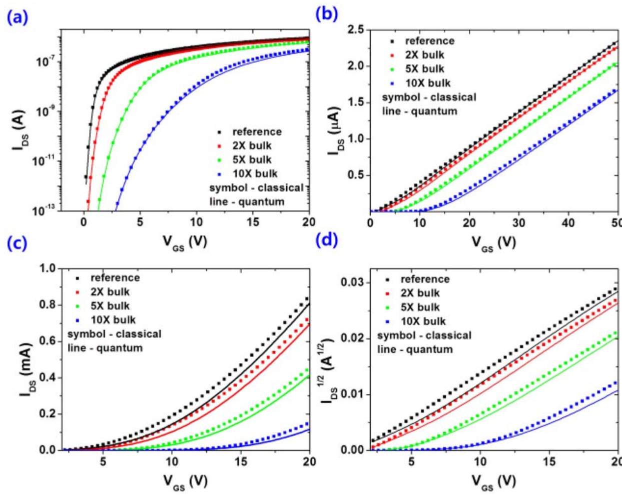

FIGURE 3. Transfer characteristics of a-IGZO TFTs with various bulk-defect DOSs plotted in the (a) logarithmic scale, (b) linear scale in the linear region ($V_{DS} = 0.01$ V), and (c) linear scale in the saturation region ($V_{DS} = 20$ V). (d) $I_{DS}^{1/2}$ *vs.* V_{GS} graph obtained from (c). The reference data were obtained using the parameters of Table 1 (bulk DOS).

on the magnitude of the bulk-defect DOS. This indicates that the shift of the threshold voltage is not related to the bulk defects but can be observed in typical TFTs that have a thin active layer when a quantum-mechanical calculation is applied.

To verify the origin of the V_{TH} shifts in the linear and saturation regions, we examined the carrier density distributions for different values of V_{DS}. Figures 4(a) and (b) show the electron density distribution of an a-IGZO TFT operating in the linear region ($V_{GS} = 20$ V, $V_{DS} = 0.01$ V), evaluated using the classical and quantum-mechanical methods, respectively. As expected, in both cases, a uniform electron density distribution is observed along the channel length direction. In this case, the difference of V_{TH} between the two methods is small.

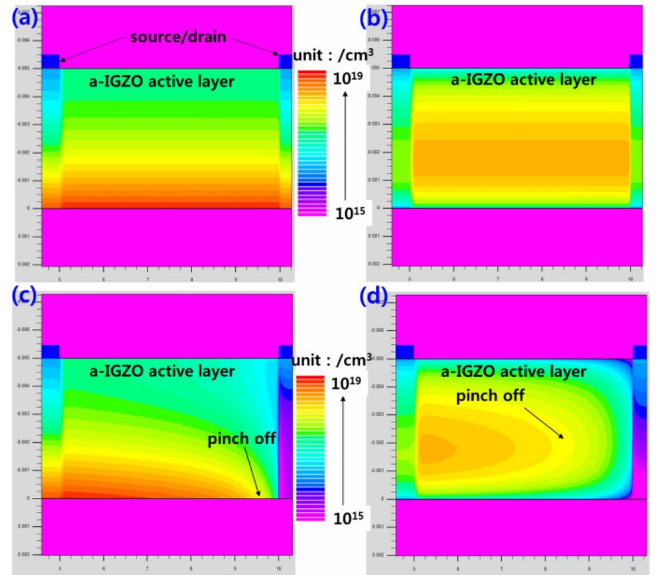

FIGURE 4. Free electron density distribution in the channel region: (a) linear region operation examined with the classical method, (b) linear region operation calculated with the quantum-mechanical method, (c) saturation region operation analyzed with the classical method, and (d) saturation region operation studied with the quantum-mechanical method. The bulk DOS was approximately 10 times the reference value. Pinch-off points were assumed when the maximum electron density was approximately 10^{18} cm^{-3} for both the classical and quantum-mechanical methods.

Figures 4(c) and (d) show the electron density distribution in the saturation region ($V_{GS} = V_{DS} = 20$ V) for the classical and quantum-mechanical methods, respectively. There are well-known pinch-off points where the channel region does not exist in the drain sides. After the formation of the pinch-off points, the electrons flow through a space-charge-limited region with high bulk resistance. In the classical calculation, most of the electrons are generated by the gate-to-source voltage in the interface region with very high electron density. Despite the application of a large V_{DS}, the high-electron-density channel region remains and compresses the space-charge-limited region, as shown in Fig. 4(c). However, in the quantum-mechanical calculation, the peak electron density is relatively low and the channel electrons show a relatively wide distribution. Therefore, the channel electrons in the drain side are further removed by the large V_{DS} and the space-charge-limited region is extended to the source side, as shown in Fig. 4(d). This leads to a positive shift of V_{TH} for operation in the saturation region when the quantum effect is considered, which differs from the classical results.

VI. EFFECTS OF INTERFACIAL DENSITY OF STATES

Next, we analyzed the effect of the interfacial states on the thin-active-layer a-IGZO TFTs. Figures 5(a) and (b) show the transfer characteristics of a-IGZO TFTs operating in the linear region for different interfacial-defect DOSs (the bulk-defect DOS is assumed to be zero). The interfacial-defect DOS varied from 1 to 10 times the reference value. When the

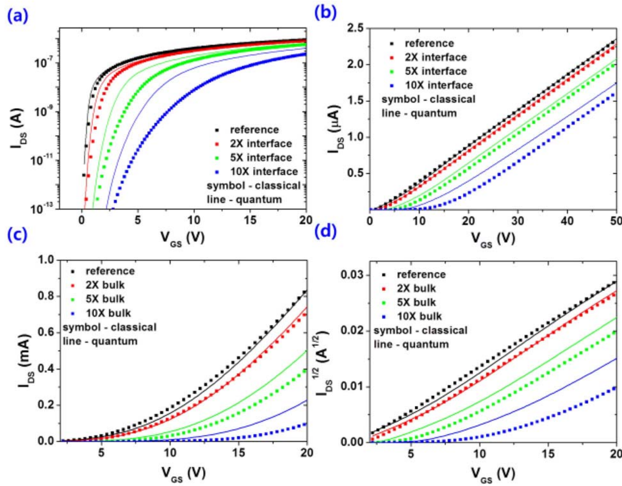

FIGURE 5. Transfer characteristics of a-IGZO TFTs with different interfacial-defect DOS plotted in the (a) logarithmic scale, (b) linear scale in the linear region ($V_{DS} = 0.01$ V), and (c) linear scale in the saturation region ($V_{DS} = 20$ V). (d) $I_{DS}^{1/2}$ *vs.* V_{GS} graph obtained from (c). The reference data were obtained using the parameters of Table 1 (interfacial DOS).

interfacial states were introduced, the classical and quantum mechanical methods obtained different transfer characteristics. Specifically, the subthreshold slopes (SS, dimension: V/dec) decreased, the field-effect mobility values increased, and the threshold voltages shifted toward the negative direction when calculated with the quantum-mechanical method, especially for high interfacial-defect DOS.

Figures 5(c) and (d) show the transfer characteristics and ${I_{DS}}^{1/2}$ *vs.* V_{GS} graphs, respectively, for various interfacial-defect DOSs. The amount of the shift of V_{TH} is closely related to the magnitude of the interfacial-defect DOS. As the interfacial-defect DOS increases, V_{TH} shifts further in the negative direction, as shown in Figs. 5(c) and (d), which is significantly different from that of the bulk-defect DOS, shown in Figs. 3(c) and (d). It is well known that when the acceptor-like defect DOS decreases, a negative shift of the threshold voltage, an increase in the field-effect mobility, and a decrease in the SS are observed. This indicates that when the quantum effect is considered, the 'effective' interfacial DOS decreases for both the deep and tail states, leading to an improvement of device performance.

This interesting behavior is closely related to the distribution of the free electron density. Figure 6 shows the distribution of the free electron density along the channel thickness direction when the number of interfacial states is 10 times higher than that of the reference sample. For the quantum-mechanical calculation, the peak point of the electron density was separated from the interface and most of the free electrons were distributed near the center of the active region. Consequently, as the electron trapping probability was relatively low when the interfacial defects were spatially separated from the channel region, the influence of the interfacial defect decreased. This lead to an increase in the free electron density for the weak accumulation condition ($V_{GS} = 5$ V and $V_{DS} = 0.01$ V), as shown in Fig. 6.

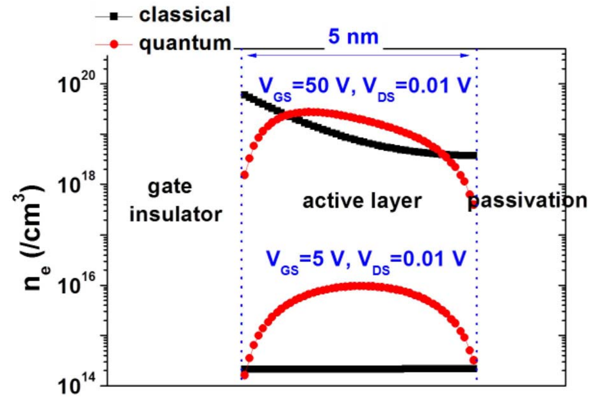

FIGURE 6. Free electron density distribution of a-IGZO TFTs along the channel thickness direction after the introduction of the interfacial-defect DOS. The defect DOS was approximately 10 times the reference value.

Note that in the strong accumulation condition (V_{GS} = 50 V, V_{DS} = 0.01 V), the difference in the electron density distribution did not induce a variation of the field-effect mobility, as shown in Fig. 5(b). The magnitude of the total free electron density and the corresponding field-effect mobility were similar for the classical and quantum-mechanical methods. The reason is that the interfacial-defect DOS is fully ionized for a large V_{GS} and the quantum-mechanical method results in a field-effect mobility similar to that of the classical method.

Experiments have observed an enhanced performance of oxide-based TFTs when an electron-confining structure is applied. Recently, Rum *et al.* [24] reported that a decrease in the SS and an increase in the field-effect mobility were observed for solution-processed amorphous ITZO–IGZO heterojunction TFTs when the confining ITZO was approximately 3 nm. It is speculated that this performance enhancement originates from the quantum-mechanical effect, which spatially separates the channel region from the interfacial-defect region. Moreover, as solution-processed TFTs typically have a significant interfacial-defect DOS compared to vacuum-processed TFTs, the performance improvement is more clearly observed in solution-processed oxide-based TFTs, which is confirmed by Figs. 5(a)–(d).

Finally, to analyze the quantum effect with the presence of both bulk and interfacial states in the a-IGZO active layer, which provides a realistic description of the device, we introduced both bulk- and interfacial-defect DOSs (5 times the reference values) and repeated the simulation. Figures 7(a) and (b) show the transfer characteristics of an a-IGZO TFT in the linear ($V_{DS} = 0.01$ V) and saturation regions ($V_{DS} = 20$ V), respectively. It can be seen that the *SS* decreased and the threshold voltage shifted in the negative direction for the quantum-mechanical method. This result is similar to that obtained when only the interfacial DOS was considered because the effect of the bulk-defect DOS is relatively small, as discussed in Section V. This indicates that the interfacial-defect DOS is the main factor that makes the quantum effect prominent for a-IGZO TFTs.

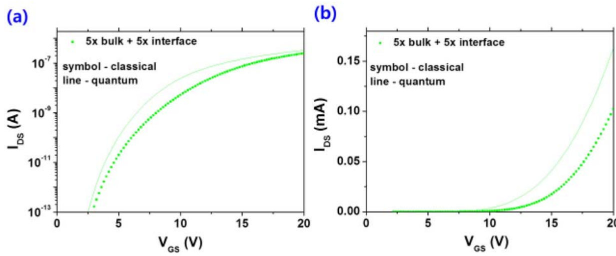

FIGURE 7. Transfer characteristics of a-IGZO TFTs with bulk and interfacial DOSs 5 times higher than the reference values operating in the (a) linear region (V_{DS} = 0.01 V), and (b) saturation region (V_{DS} = 20 V).

Therefore, to characterize the performance of a-IGZO TFTs with nanometer-scale active layers, the quantum effect must be considered, especially for the interfacial-defect DOS.

VII. CONCLUSION

In conclusion, a-IGZO TFTs with a thin active layer were simulated using the classical and quantum-mechanical methods for bulk and interfacial DOS. For the bulk-defect DOS, a positive shift in the threshold voltage was observed with the quantum mechanical method, compared to that calculated with the classical method for the saturation region operation, because of the formation of a long space-charge-limited region. The shift was independent of the magnitude of the bulk-defect DOS. On the other hand, for the interfacial-defect DOS, the quantum-mechanical method showed a decrease in the SS and a negative shift in the threshold voltage, compared to those derived with the classical method in the linear and saturation regions, as the free electron density distribution was separated from the interfacial region when the quantum effect was considered. These variations were dependent on the magnitude of the interfacial-defect DOS. Therefore, it is important to consider the quantum-mechanical effect when characterizing the electrical properties of amorphous oxide-based TFTs with thin active layers. In particular, an accurate analysis of the effect of the defect density in oxide-based TFTs is possible only by considering the quantum effect.

ACKNOWLEDGMENT

The author thanks to Mr. Seungwoon Lee for his help in data collection.

REFERENCES

[1] K. Nomura *et al.*, "Room-temperature fabrication of transparent flexible thin-film transistors using amorphous oxide semiconductors," *Nature*, vol. 432, no. 7016, pp. 488–492, 2004.
[2] S. Masuda *et al.*, "Transparent thin film transistors using ZnO as an active channel layer and their electrical properties," *J. Appl. Phys.*, vol. 93, no. 3, pp. 1624–1630, 2003.
[3] T. Hirano *et al.*, "Bottom-gate zinc oxide thin-film transistors (ZnO TFTs) for AM-LCDs," *IEEE Trans. Electron Devices*, vol. 55, no. 11, pp. 3136–3142, Nov. 2008.
[4] T.-C. Fung *et al.*, "Two-dimensional numerical simulation of radio frequency sputter amorphous In-Ga-Zn-O thin-film transistors," *J. Appl. Phys.*, vol. 106, no. 8, pp. 1–10, 2009.
[5] C. Zhao, L. Bie, R. Zhang, and J. Kanicki, "Two-dimensional numerical simulation of bottom-gate and dual-gate amorphous In-Ga-Zn-O MESFETs," *IEEE Electron Device Lett.*, vol. 35, no. 1, pp. 75–77, Jan. 2014.
[6] H.-H. Hsieh, T. Kamiya, K. Nomura, H. Hosono, and C.-C. Wu, "Modeling of amorphous InGaZnO4 thin film transistors and their subgap density of states," *Appl. Phys. Lett.*, vol. 92, no. 13, pp. 1–3, 2008.
[7] D. H. Kim *et al.*, "Physical parameter-based SPICE models for InGaZnO thin-film transistors applicable to process optimization and robust circuit design," *IEEE Electron Device Lett.*, vol. 33, no. 1, pp. 59–61, Jan. 2012.
[8] M. Mativenga, D. Geng, J. H. Chang, T. J. Tredwell, and J. Jang, "Performance of 5-nm a-IGZO TFTs with various channel lengths and an etch stopper manufactured by back UV exposure," *IEEE Electron Device Lett.*, vol. 33, no. 6, pp. 824–826, Jun. 2012.
[9] J.-H. Kim, J. Kim, S. M. Jeong, and J. Jeong, "Storage-period dependent bias-stress instability of solution-processed amorphous indium–zinc-oxide thin-film transistors," *Current Appl. Phys.*, vol. 15, pp. S64–S68, Sep. 2015.
[10] D. Connelly, Z. Yu, and D. Yergeau, "Macroscopic simulation of quantum mechanical effects in 2-D MOS devices via the density gradient method," *IEEE Trans. Electron Devices*, vol. 49, no. 4, pp. 619–626, Apr. 2002.
[11] N.-M. Park, C.-J. Choi, T.-Y. Seong, and S.-J. Park, "Quantum confinement in amorphous silicon quantum dots embedded in silicon nitride," *Phys. Rev. Lett.*, vol. 86, no. 7, pp. 1355–1357, 2001.
[12] N.-M. Park, T.-S. Kim, and S.-J. Park, "Band gap engineering of amorphous silicon quantum dots for light-emitting diodes," *Appl. Phys. Lett.*, vol. 78, no. 17, pp. 2575–2577, 2001.
[13] L. D. Negro *et al.*, "Light emission from silicon-rich nitride nanostructures," *Appl. Phys. Lett.*, vol. 88, Feb. 2006, Art. no. 183103.
[14] G. Allan, C. Delerue, and M. Lannoo, "Electronic structure of amorphous silicon nanoclusters," *Phys. Rev. Lett.*, vol. 78, no. 16, pp. 3161–3164, 1997.
[15] Y. Omura, S. Horiguchi, M. Tabe, and K. Kishi, "Quantum-mechanical effects on the threshold voltage of ultrathin-SOI nMOSFETs," *IEEE Electron Device Lett.*, vol. 14, no. 12, pp. 569–571, Dec. 1993.
[16] F. Assad, Z. Ren, D. Vasileska, S. Datta, and M. Lundstrom, "On the performance limits for Si MOSFETs: A theoretical study," *IEEE Trans. Electron Devices*, vol. 47, no. 1, pp. 232–240, Jan. 2000.
[17] A. Wettstein, A. Schenk, and W. Fichtner, "Quantum device-simulation with the density-gradient model on unstructured grids," *IEEE Trans. Electron Devices*, vol. 48, no. 2, pp. 279–284, Feb. 2001.
[18] A. Asenov, G. Slavcheva, A. R. Brown, J. H. Davies, and S. Saini, "Increase in the random dopant induced threshold fluctuations and lowering in sub-100 nm MOSFETs due to quantum effects: A 3-D density-gradient simulation study," *IEEE Trans. Electron Devices*, vol. 48, no. 4, pp. 722–729, Apr. 2001.
[19] A. Asenov, G. Slavcheva, A. R. Brown, J. H. Davies, and S. Saini, "Quantum mechanical enhancement of the random dopant induced threshold voltage fluctuations and lowering in sub 0.1 micron MOSFETs," in *Int. Electron Devices Metting Tech. Dig.*, Washington, DC, USA, 1999, pp. 535–538.
[20] H. Yabuta *et al.*, "High-mobility thin-film transistor with amorphous in Ga Zn O_4 channel fabricated by room temperature rf-magnetron sputtering," *Appl. Phys. Lett.*, vol. 89, Jul. 2006, Art. no. 112123.
[21] J. Jeong, J. Kim, and S. M. Jeong, "Novel gated-multiprobe method for measuring a back electrode effect in amorphous oxide-based thin-film transistors," *IEEE Trans. Electron Devices*, vol. 61, no. 11, pp. 3757–3761, Nov. 2014.
[22] A. Takagi *et al.*, "Carrier transport and electronic structure in amorphous oxide semiconductor, a-$InGaZnO_4$," *Thin Solid Films*, vol. 486, nos. 1–2, pp. 38–41, 2005.
[23] J. Jeong and Y. Hong, "Debye length and active layer thickness-dependent performance variations of amorphous oxide-based TFTs," *IEEE Trans. Electron Devices*, vol. 59, no. 3, pp. 710–714, Mar. 2012.
[24] Y. S. Rim *et al.*, "Boost up mobility of solution-processed metal oxide thin-film transistors via confining structure on electron pathways," *Adv. Mater.*, vol. 26, no. 25, pp. 4273–4278, 2014.

JAEWOOK JEONG, photograph and biography not available at the time of publication.